Optics Letters

Instant and efficient second-harmonic generation and downconversion in unprepared graded-index multimode fibers

M. A. Eftekhar,[1,*] Z. Sanjabi-Eznaveh,[1] J. E. Antonio-Lopez,[1] F. W. Wise,[2] D. N. Christodoulides,[1] and R. Amezcua-Correa[1]

[1]CREOL, College of Optics and Photonics, University of Central Florida, Orlando, Florida 32816-2700, USA
[2]School of Applied and Engineering Physics, Cornell University, Ithaca, New York 14853, USA
*Corresponding author: m.a.eftekhar@knights.ucf.edu

Received 25 May 2017; revised 19 July 2017; accepted 19 July 2017; posted 31 July 2017 (Doc. ID 295880); published 30 August 2017

We show that germanium-doped graded-index multimode silica fibers can exhibit relatively high conversion efficiencies (~6.5%) for second-harmonic generation when excited at 1064 nm. This frequency-doubling behavior is also found to be accompanied by an effective downconversion. As opposed to previous experiments carried out in single- and few-mode fibers where hours of preparation were required, in our system, these $\chi^{(2)}$ related processes occur almost instantaneously. The efficiencies observed in our experiments are, to the best of our knowledge, among the highest ever reported in unprepared fibers.

OCIS codes: (060.4370) Nonlinear optics, fibers; (190.2620) Harmonic generation and mixing; (190.4223) Nonlinear wave mixing; (190.4380) Nonlinear optics, four-wave mixing.

https://doi.org/10.1364/OL.42.003478

Second-harmonic generation (SHG) in silica single-mode optical fibers was first reported by Österberg and Margulis [1,2]. This was quite surprising given that amorphous systems like silica glass are not expected to exhibit a $\chi^{(2)}$ nonlinearity. This, in turn, incited considerable interest in the physics and applications of these effects, especially in single-mode fibers [3–8]. In early experiments, SHG was observed only after preparing the fiber by exposing it to the pump wavelength for several hours. While this process still remains poorly understood, a number of schemes have proved effective in increasing its conversion efficiency and reducing the required preparation time. Such techniques include, for example, seeding a fiber with a second-harmonic (SH) signal along with the pump light [3], using polling techniques like thermal [9,10] and corona poling [11], and applying a transverse dc electric field in order to break the inversion symmetry of the material system [5]. Electron implantation was also utilized along similar lines [12]. It is important to note that most of these experiments were conducted primarily in single-mode or few-mode fibers where only the fundamental mode was excited [13].

Quite recently, multimode fibers (MMFs) have made a strong comeback in multichannel communication systems when used in conjunction with spatial division multiplexing [14]. In parallel to these activities, there has been also a resurgence of interest in their nonlinear properties [15–23]. In principle, their larger cross section can be exploited to generate power spectral densities that are orders of magnitudes higher than those expected from single-mode fibers [20]. In addition, the many degrees of freedom provided by these highly multimoded structures can be exploited to tailor, at will, their output frequency content [24,25]. In this respect, geometric parametric instabilities (GPIs) and beam cleaning were observed for the first time in parabolic-index MMFs [20,26]. Second-harmonic generation was also recently observed along with their GPI sidebands in optically polled graded-index multimode fibers [27]. In this study, the fiber was first prepared by exposing it for a few minutes to a second-harmonic signal generated from a KTP crystal. Subsequently, SHG conversion up to 1% was reported a few hours after the fiber was prepared.

Here, we experimentally demonstrate high SHG conversion efficiencies (~6.5%) in heavily multimode parabolic-index germanium-doped optical fibers. Unlike previous studies, this conversion occurred without first preparing the fiber via any of the schemes outlined before. Even more importantly, the SHG was found to reach a maximum in an almost instantaneous manner. In our experiments, this frequency-doubling was also accompanied by an efficient downconversion process in the near-IR regime (2128 nm). The effect of input pump power on the efficiency of these processes was also investigated. Cutback measurements performed on our fiber revealed that SHG effectively unfolded along the first 4–5 m. In all cases, the recorded output beam profiles (pump and SH) were found to exhibit a Gaussian-like shape and a speckle-free pattern.

A schematic representation of the experimental setup used is depicted in Fig. 1. The optical source is an amplified *Q*-switched microchip laser, producing 400 ps pulses at a repetition rate of 500 Hz and with peak powers up to 200 kW.

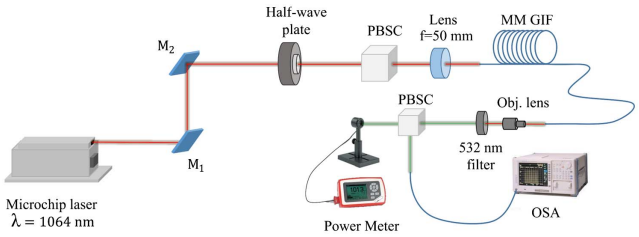

Fig. 1. Schematic of the setup used for SHG and downconversion in MMFs. Pulses from a *Q*-switched microchip laser at 1064 nm are coupled into a MMF. PBSC, polarizing beam splitter cube; M1 and M2, Mirrors; OSA, optical spectrum analyzer.

Each pulse carries 95 μJ of energy at 1064 nm. The laser beam is coupled to the multimode fiber samples using a 50 mm focal length lens with efficiencies exceeding 80%. To control the input power, a half-wave plate and a polarizing beam splitter cube were employed. The fiber was fixed on a three-axis translation stage. The visible and NIR portions of the output spectra were collected by a multimode patch cord and were analyzed using two different optical spectrum analyzers covering the wavelength range from 350 to 1750 nm (*ANDO AQ 6315E*) and 1200 to 2400 nm (*Yokogawa AQ6375*). To record the beam profile of the second-harmonic signal, a CCD camera was used along with a 532 nm filter having 10 nm FWHM. In our experiments, two different MMFs were utilized. The first one was a low differential modal group delay multimode graded-index fiber with a core diameter of 50 μm and a refractive index contrast of $\sim 1.6 \times 10^{-2}$. The second MMF was of the step-index type having a numerical aperture of 0.22 and a core diameter of 105 μm. Both these fibers were germanium-doped and fabricated by Prysmian Group. At 1064 nm, the parabolic MMF used is expected to support ~250 modes while at 532 it is expected to support ~1000 modes.

The output spectra, collected at the end of a 5 m long parabolic-index MMF, are depicted in Fig. 2 for three different input power levels. Figure 2(a) shows the spectrum when the average input power is ~16 mW ($P_{p-p} = 80$ kW). In addition to pump and Raman sidebands, a distinct peak at 532 nm is clearly visible—signifying the onset of SHG. This peak is accompanied by another rather strong line located at 560 nm, resulting from the frequency-doubling of the first Stokes Raman peak (R_1) at 1.118 μm. As can be seen in Fig. 2(b), by increasing the input power, a few other peaks start to appear in the vicinity of the pump's second harmonic. In particular, the line at 587 nm corresponds to the frequency-doubling of the second Stokes Raman wave at 1.176 μm. In addition, two other peaks can be prominently seen at 546 nm and 577 nm. The first one can be attributed to a sum-frequency generation of the pump and the first Stokes peak, while the second one can be attributed to a sum-frequency generation resulting from the first and second Stokes Raman peaks. This clearly indicates that the $\chi^{(2)}$ response of the fiber is indeed at play. Other significant frequency peaks appearing around 720 nm correspond to sidebands generated from GPI that takes place in parabolic multimode fibers, as also demonstrated in previous studies [19,20]. It should be noted that the distinct feature seen at 806 nm is the residual pump from our laser. By further raising the input power, a series of peaks starts to emerge between 420 and 490 nm, which can be ascribed to sum-frequency generation

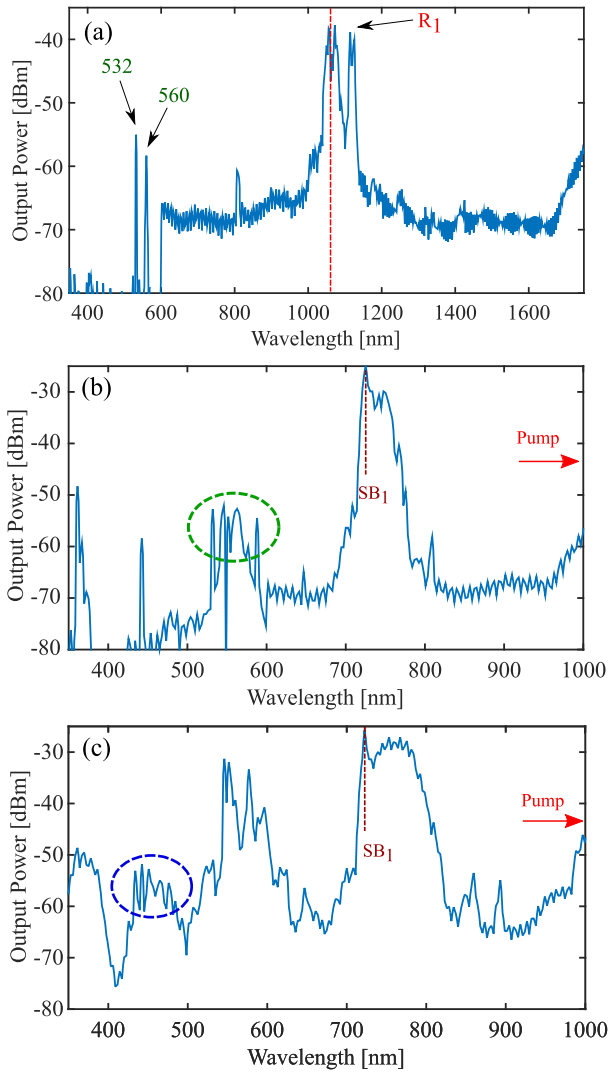

Fig. 2. (a) Output spectrum measured at the end of a 5 m long parabolic MMF when excited with 400 ps 80 kW peak power pulses. SHG from the pump is evident at 532 nm. The line at 560 nm is due to the frequency-doubling of first Stokes Raman wave. (b) Increasing the input pump power to 110 kW results in the appearance of extra peaks in the vicinity of 532 nm (green cluster). (c) A further increase in the input pump power to 140 kW leads to other $\chi^{(2)}$ induced peaks in the 420–490 nm (blue cluster) wavelength range. SB_1 represents the first GPI sideband.

between the pump or the Raman peaks and the first visible GPI sideband located at 720 nm [Fig. 2(c)].

We would like to note that these lines do not result from any GPI sideband generation at 532 nm, as evidenced from the fact that they only appear on the higher frequency side of the second harmonic (i.e., the generation is not symmetric). In all cases, we found that the power in the SH signal depends on the initial launching conditions, thus allowing one to optimize the SHG conversion by tuning the input (i.e., by selecting appropriate mode groups). In that case, the multiplicity of modes involved can always allow for phase matching to occur between different mode groups in a very large number of ways. In general, SHG in multimode systems can result either from the

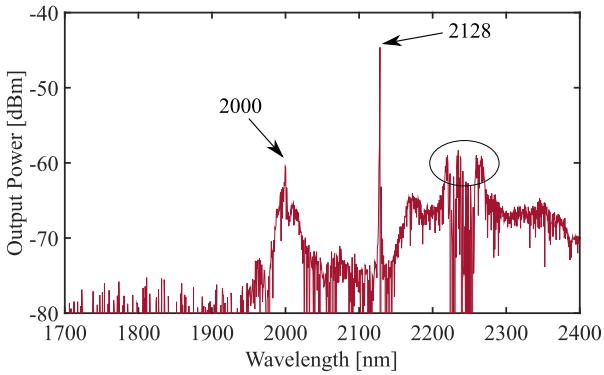

Fig. 3. NIR portion of the spectrum collected at the end of a 5 m long parabolic MMF when pumped at 110 kW peak power. The prominent peak at 2128 corresponds to the pump downconversion. The peak at 2 μm results from the first NIR GPI sideband.

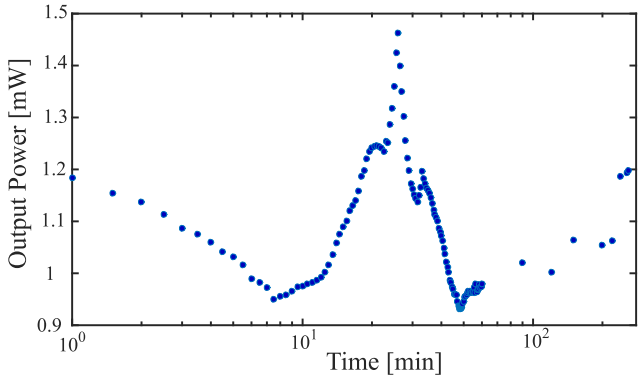

Fig. 4. Temporal evolution of the generated second harmonic, measured at the output of a 5 m long GI-MMF. The peak power used was 110 kW. The measurements were carried out for over 4 h. Once the oscillations settle down, the SH power level is restored to its initial value.

same pump mode ($2\beta^{(\omega)}_{(m,n)} = \beta^{(2\omega)}_{(k,l)}$) or from two different modes carrying the pump ($\beta^{(\omega)}_{(m,n)} + \beta^{(\omega)}_{(i,j)} = \beta^{(2\omega)}_{(k,l)}$) [28].

Figure 3 shows the NIR portion of the spectrum, which also displays a series of peaks. The strongest line in this region is located at 2.128 μm, corresponding to the downconverted wavelength of the pump, generated along with the second harmonic because of the $\chi^{(2)}$ nonlinearity. Our experiments revealed that any change in the power level of the produced SH was always accompanied by a similar change in the downconverted signal. Another significant feature in this figure is the spectral band around 2 μm. This line corresponds to the first NIR-GPI sideband. Some of the spectral components between 2.13 and 2.35 μm also match the downconversion of the first Stokes Raman waves.

As a next step, we repeated these experiments in the previously mentioned step-index MMF. Even in this case, the presence of the second harmonic was evident in the spectrum. However, our measurements showed that the generated green light (SH) was always very weak, by almost 2 orders of magnitude below that observed in the parabolic fiber. Further increasing the input pump power or prolonging the exposure time of this step-index MMF to the pump did very little in enhancing the generated SH signal. The same is also true for the downconverted wavelength. One possible explanation behind this difference in performance can be attributed to the GPI process that is only possible in parabolic fibers. One of the direct byproducts of GPI is the generation of strong lines both in the visible as well as the UV part of the spectrum. As has been shown before, exposing the fiber to green, blue, or the UV wavelengths can enhance SHG up to 10 times [29]. As a result, in our experiments, the GPI-induced wavelengths in the red/blue may act as enabling sources in "preparing" the fiber toward generating more efficiently the SH and downconverted signals.

A surprising result in our experiments was the fact that SHG occurred almost instantaneously in the parabolic MMF—even in the absence of any preparation. Figure 4 demonstrates the evolution of the generated SH in a 5 m long parabolic fiber as a function of time. A 532 nm bandpass filter was used to select the second-harmonic signal. The ensued SHG was monitored for 4 h. The pump signal was initially blocked for a few minutes before initiating these measurements. As soon as the pump was unblocked, green light at 532 nm always emerged and was measured using a power meter. To make sure that this instant SHG does not result from any previous exposure of the fiber to the pump, we repeated this same experiment with totally unexposed fiber segments. In all cases, SHG took place almost immediately after the laser beam was coupled into the fiber. As can be seen in Fig. 4, the SH output power experiences fluctuations during the first few minutes. Our observations indicate that these oscillations become progressively less pronounced and as a result, the output SH slowly stabilizes around its initial value. It is worth mentioning that these fluctuations (±10%) are always present. This behavior can be explained by considering the continuous formation and erasure of internal gratings induced by the co-propagating GPI-sideband colors. The reason behind this instant buildup of the $\chi^{(2)}$ process is still unclear to us.

In another set of experiments, we investigated the dependence of the conversion efficiency on the input pump power. These studies were conducted again in a 5 m long parabolic MMF. These results are shown in Fig. 5. For each power level, the initial conditions were tuned to yield the highest attainable SHG efficiency. As demonstrated in this figure, the efficiency of this process tends to monotonically increase with pump power. However, once the average input powers exceeds 20 mW ($\sim P_{p\text{-}p} = 100$ kW) the SHG saturates and hence

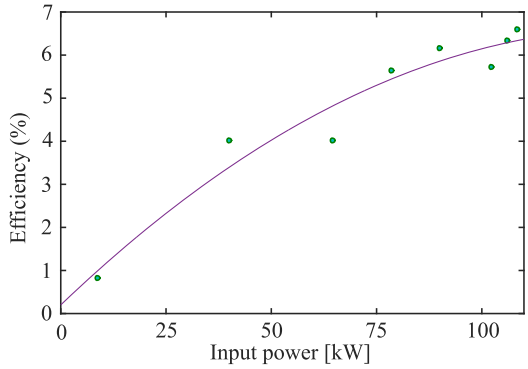

Fig. 5. Output power conversion SH efficiency measured at the end of a 5 m long GI-MMF. The SHG monotonically increases with the pump power. The process saturates at 100 kW.

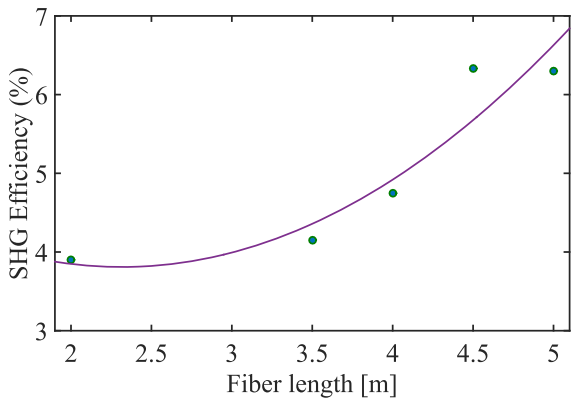

Fig. 6. Power conversion efficiency for different fiber lengths. The efficiency tends to increase with distance in the parabolic MMF.

the efficiency no longer changes. In this regime, the maximum achievable peak power conversion was found to be 6.5%, which, to the best of our knowledge, is among the highest observed in unprepared fibers.

The effect of fiber length on the SHG process was previously investigated in single-mode fibers. In these studies, it was found that only the first few tens of centimeters are responsible for SHG [1]. Here, we probed the same behavior in parabolic MMFs having different lengths. These results are depicted in Fig. 6. As opposed to single-mode fibers, in our case, we found that the SHG kept increasing with distance, way beyond the first 50 cm (Fig. 6), and it only seems to saturate after 4.5 m.

The output beam profile distributions at the pump wavelength and SH (532 nm) are plotted in Fig. 7 for different pump power levels. In accord with previous observations [20,26], the beam at the pump wavelength was found to be clean and speckle-free. Similarly, the beam profile for the SH 532 nm line had a Gaussian-like shape and was again speckle-free, a surprising result given the low power levels at SH (532 nm). This may be due to the fact the pump clean-up, in turn, induces a similar effect in the SH, i.e., by populating lower-order modes.

In conclusion, we have shown that germanium-doped parabolic multimode silica fibers can exhibit relatively high SHG conversion efficiencies and downconversion. Unlike previous experiments, these $\chi^{(2)}$ related processes occurred immediately without any preparation. Of interest would be to consider the potential of the $\chi^{(2)}$ downconversion process as a source for biphoton generation in quantum optics. Our results may pave the way toward alternative platforms for SHG and downconversion.

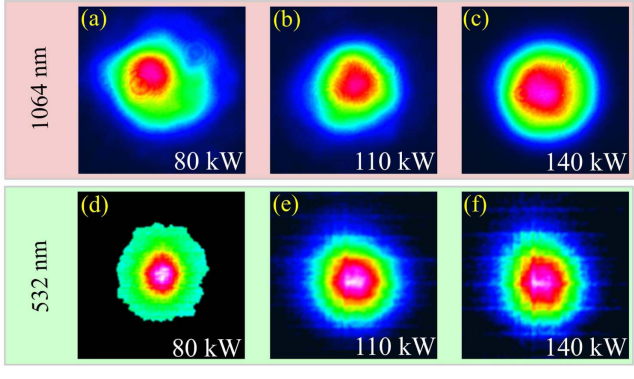

Fig. 7. Output beam profile at (a)–(c) 1064 nm and (d)–(f) 532 nm after a 5 m long parabolic MMF, as a function of input power.

Funding. Office of Naval Research (ONR) (MURI N00014-13-1-0649); HEL-JTO (W911NF-12-1-0450); Army Research Office (ARO) (W911NF-12-1-0450); Air Force Office of Scientific Research (AFOSR) (FA9550-15-10041); Qatar National Research Fund (QNRF) (NPRP 9-020-1-006).

REFERENCES

1. U. Österberg and W. Margulis, Opt. Lett. **11**, 516 (1986).
2. W. Margulis and U. Österberg, J. Opt. Soc. Am. B **5**, 312 (1988).
3. R. H. Stolen and H. W. K. Tom, Opt. Lett. **12**, 585 (1987).
4. R. W. Terhune and D. A. Weinberger, J. Opt. Soc. Am. B **4**, 661 (1987).
5. M.-V. Bergot, M. C. Farries, M. E. Fermann, L. Li, L. J. Poyntz-Wright, P. St.J. Russell, and A. Smithson, Opt. Lett. **13**, 592 (1988).
6. F. Ouellette, K. O. Hill, and D. C. Johnson, Opt. Lett. **13**, 515 (1988).
7. V. Mizrahi, Y. Hibino, and G. Stegeman, Opt. Commun. **78**, 283 (1990).
8. D. Z. Anderson, V. Mizrahi, and J. E. Sipe, Opt. Lett. **16**, 796 (1991).
9. P. G. Kazansky, L. Dong, and P. St.J. Russell, Opt. Lett. **19**, 701 (1994).
10. V. Pruneri, G. Bonfrate, P. G. Kazansky, D. J. Richardson, N. G. Broderick, J. P. D. Sandro, C. Simonneau, P. Vidakovic, and J. A. Levenson, Opt. Lett. **24**, 208 (1999).
11. A. Okada, K. Ishii, K. Mito, and K. Sasaki, Appl. Phys. Lett. **60**, 2853 (1992).
12. P. G. Kazansky, A. Kamal, and P. St.J. Russell, Opt. Lett. **18**, 693 (1993).
13. M. A. Saifi and M. J. Andrejco, Opt. Lett. **13**, 773 (1988).
14. D. J. Richardson, J. M. Fini, and L. E. Nelson, Nat. Photonics **7**, 354 (2013).
15. W. H. Renninger and F. W. Wise, Nat. Commun. **4**, 1719 (2013).
16. L. G. Wright, D. N. Christodoulides, and F. W. Wise, Nat. Photonics **9**, 306 (2015).
17. L. G. Wright, W. H. Renninger, D. N. Christodoulides, and F. W. Wise, Opt. Express **23**, 3492 (2015).
18. H. Pourbeyram, G. P. Agrawal, and A. Mafi, Appl. Phys. Lett. **102**, 201107 (2013).
19. K. Krupa, A. Tonello, A. Barthélémy, V. Couderc, B. M. Shalaby, A. Bendahmane, G. Millot, and S. Wabnitz, Phys. Rev. Lett. **116**, 183901 (2016).
20. G. Lopez-Galmiche, Z. Sanjabi Eznaveh, M. A. Eftekhar, J. Antonio Lopez, L. G. Wright, F. Wise, D. Christodoulides, and R. Amezcua Correa, Opt. Lett. **41**, 2553 (2016).
21. F. Poletti and P. Horak, Opt. Express **17**, 6134 (2009).
22. L. G. Wright, Z. Liu, D. A. Nolan, M.-J. Li, D. N. Christodoulides, and F. W. Wise, Nat. Photonics **10**, 771 (2016).
23. E. Nazemosadat, H. Pourbeyram, and A. Mafi, J. Opt. Soc. Am. B **33**, 144 (2016).
24. Z. S. Eznaveh, M. A. Eftekhar, J. E. A. Lopez, M. Kolesik, A. Schülzgen, F. W. Wise, D. N. Christodoulides, and R. A. Correa, Opt. Lett. **42**, 1015 (2017).
25. M. A. Eftekhar, L. G. Wright, M. S. Mills, M. Kolesik, R. A. Correa, F. W. Wise, and D. N. Christodoulides, Opt. Express **25**, 9078 (2017).
26. K. Krupa, A. Tonello, B. M. Shalaby, M. Fabert, A. Barthélémy, G. Millot, S. Wabnitz, and V. Couderc, Nat. Photonics **11**, 237 (2017).
27. D. Ceoldo, K. Krupa, A. Tonello, V. Couderc, D. Modotto, U. Minoni, G. Millot, and S. Wabnitz, Opt. Lett. **42**, 971 (2017).
28. W. Nakagawa, R.-C. Tyan, and Y. Fainman, J. Opt. Soc. Am. A **19**, 1919 (2002).
29. T. J. Driscoll and N. M. Lawandy, Opt. Lett. **17**, 571 (1992).